# Attosecond-pump attosecond-probe x-ray spectroscopy of liquid water

Shuai Li,[1,†] Lixin Lu,[2,†] Swarnendu Bhattacharyya,[3,†] Carolyn I. Pearce,[4] Kai Li,[1,5] Emily T. Nienhuis,[4] Gilles Doumy,[1] R.D. Schaller,[6] S. Moeller,[7] M.-F. Lin,[7] G. Dakovski,[7] D.J. Hoffman,[7] D. Garratt,[8] Kirk A. Larsen,[8] J.D. Koralek,[7] C.Y. Hampton,[7] D. Cesar,[7] Joseph Duris,[7] Z. Zhang,[7] Nicholas Sudar,[7] James P. Cryan,[7,8] A. Marinelli,[7,8] Xiaosong Li,[2*] Ludger Inhester,[3,9] Robin Santra,[3,9,10*] Linda Young[1,5*]

[1]Chemical Sciences and Engineering Division, Argonne National Laboratory, Lemont, IL USA

[2]Department of Chemistry, University of Washington, Seattle, WA, USA

[3]Center for Free-Electron Laser Science CFEL,
Deutsches Elektronen-Synchrotron DESY, Hamburg, Germany

[4]Pacific Northwest National Laboratory, Richland, WA, USA

[5]Department of Physics and James Franck Institute, The University of Chicago, Chicago, IL, USA

[6]Center for Nanoscale Materials, Argonne National Laboratory, Lemont, IL, USA

[7]SLAC National Accelerator Laboratory, Menlo Park, CA, USA

[8]Stanford PULSE Institute, SLAC National Accelerator Laboratory, Menlo Park, CA, USA

[9]The Hamburg Centre for Ultrafast Imaging, Hamburg, Germany

[10]Department of Physics, Universität Hamburg, Hamburg, Germany

[†]These authors contributed equally.

[*]To whom correspondence should be addressed

e-mail: young@anl.gov, robin.santra@cfel.de, xsli@uw.edu

**One sentence summary:** Attosecond x-rays freeze hydrogen atom motion to capture the incipient electronic response in radiolysis and the structure of liquid water.

**Attosecond-pump/attosecond-probe experiments have long been sought as the most straightforward method to observe electron dynamics in real time. While numerous attosecond science successes have been achieved with overlapped near infrared femtosecond and extreme ultraviolet attosecond pulses combined with sophisticated theory, true attosecond-pump/attosecond-probe experiments have been limited due to the low intensity of commonly available attosecond pulses. We use a tunable, synchronized attosecond x-ray pulse pair from an x-ray free electron laser to study the initial electronic response to valence ionization in liquid water via all x-ray attosecond transient absorption spectroscopy (AX-ATAS). Our analysis shows that the AX-ATAS response is confined to the subfemtosecond timescale, thus eliminating any hydrogen atom motion and allowing us to demonstrate experimentally that the $1b_1$ splitting in the x-ray emission spectrum is not evidence for the existence of two structural motifs of liquid water at room temperature.**

The advent of attosecond light pulses more than twenty years ago (*1, 2*) has revolutionized ultrafast science - making it possible, in principle, to observe pure electronic dynamics free from nuclear motion. Attosecond light pulses have enabled researchers to address topics previously out of reach, most notably the timescale for photoemission - a process that had been assumed to be instantaneous. Delayed photoemission has been extensively researched in atoms (*3, 4*), molecules (*5, 6*), liquids (*7*) and solids (*8*) - with the experimental-theoretical disagreement for the simplest case of $2s$ and $2p$ photoemission time delays in gaseous neon only recently resolved (*4*). Beyond photoemission delays, attosecond methods have pioneered research ranging from the fundamental, e.g. probing the electronic response to sudden ionization (*9, 10*), charge localization and migration in molecules (*11, 12*), controlling autoionization absorption lineshapes (*13*), to the application-oriented, e.g. demonstration of reversible field control of

conductivity in dielectrics that could provide a route to ultrafast lightwave electronics (*14*).

Attosecond studies generally employ light pulses generated via high harmonic generation (HHG) starting with tabletop intense near-infrared (NIR) sources and exploit the natural synchronization between the generating and high-harmonic pulses to achieve sub-femtosecond time-resolution with spatially overlapped, time-delayed pulses (*15*). Because this experimental configuration often limits the time resolution to the cross-correlation between the NIR and HHG pulses, i.e. a few femtoseconds, or to the investigation of NIR-induced processes over short time periods via attoclock methods (*16*), and, because the NIR does not allow atomic site-selectivity in excitation or probing, all attosecond-pump/attosecond-probe experiments have been long sought (*17–20*). Unfortunately poor conversion efficiency results in only fJ to nJ HHG energies in the extreme ultraviolet (EUV), such that only a few all-attosecond pump/probe experiments have been performed (*18, 19*), with such capabilities far from routine or widely available. Moreover, despite significant advances in HHG production of x rays in the water window (*21*), tabletop all x-ray attosecond-pump/attosecond-probe experiments have not been realized. Advances in x-ray free-electron laser (XFEL) technology demonstrating attosecond hard and soft x-ray pulses (*22, 23*) with multi-$\mu$J energies are a promising alternative. Such studies represent the next step in the quest to observe electronic processes in real-time, presenting significant challenges both experimental, stemming from the production and synchronization of attosecond x-ray pulse pairs, and theoretical, associated with the understanding of the target response to combined/overlapping x-ray pump/probe fields that access core-excited states where potential energy surfaces are largely uncharacterized (*17*).

Here we report the first all-x-ray attosecond–pump/attosecond–probe study on a condensed-phase system, liquid water. Liquid water is universally important as the most common liquid on earth and essential for life; understanding the structural origin of its anomalous behavior remains a fundamental challenge (*24*) and understanding its response to ionizing radiation,

i.e. radiolysis (*25, 26*), is of importance in many fields including space travel (*27*), human health (*28*), corrosion in nuclear reactors and radioactive waste processing (*29*). Our study was enabled by the availability of intense attosecond-synchronized multicolor x-ray pulses from the LCLS's $\omega/2\omega$ XLEAP mode (*23, 30*). We employ the powerful technique of attosecond transient absorption spectroscopy (ATAS), first introduced to study valence electron motion induced by strong-field ionization of gas-phase krypton (*9*) and now a workhorse in chemical dynamics (*13, 31, 32*). ATAS is experimentally straightforward: a pump pulse excites the sample followed by a time-delayed spatially overlapped, broadband attosecond probe pulse that is spectrally dispersed onto a detector. The geometry allows the simultaneous characterization of both fast dynamics and narrow spectral features without violating any Fourier transform limits. The distinguishing feature of this study is that attosecond x-ray pulses are used both as pump and probe - and we call this method AX-ATAS, for all-x-ray attosecond transient absorption spectroscopy. As the first such experiment in condensed phase, it was imperative to establish the nature of the observed transient absorption signal. Despite potential complications, such as collisional ionization and electronic coherences, that can affect the observed polarization response of the medium, we found that, unlike the gas-phase isolated-molecule response, the condensed phase AX-ATAS signal response is confined to the attosecond timescale, i.e. much shorter than the oxygen 1s core-hole lifetime of $\sim 4$ fs. The highly localized temporal response eliminates hydrogen atom motion, allowing us to understand the observed spectrum using static geometries. Importantly, by performing the measurement before even protons have any time to move, we find experimental evidence for the fact that what is seen in x-ray emission spectroscopy (XES) as an outer-valence ($1b_1$) double-peak structure (*33, 34*) is a consequence of proton motion in inner-shell-excited states; only a single $1b_1$ peak is seen when proton motion is suppressed. This observation does not support the idea that the $1b_1$ double-peak structure signals the presence of two competing structural motifs in liquid water at room temperature and

addresses long-standing debate surrounding the intepretation of XES in liquid water (*33–38*). These two structural motifs have been suggested to exist at ambient conditions (*24*) as a persistence of the two phases of supercooled liquid water in "no man's land" (*39–43*).

The concept of our AX-ATAS experiment is shown in Figure 1. The pump pulse ($\omega$) has sufficient energy to ionize an electron from anywhere within the valence band of liquid water and the probe pulse ($2\omega$) scans the region near the oxygen K-edge (510 - 540 eV), where the absorption signatures of holes from the $1b_1$, $3a_1$, and $1b_2$ bands and equilibrium liquid water will appear. (The transition $1a_1 \rightarrow 2a_1$ is dipole forbidden.) Since the pump pulse has energy between 255-270 eV, ionization from the valence band orbital leads to ejected photoelectrons with kinetic energies $> 200$ eV that are sufficient to further ionize water molecules on the subfemtosecond timescale, as shown in Fig. 1B. The XLEAP mode of operation at LCLS (*23*) was used to produce two attosecond pulses of $\sim 600$-as duration whose photon energies are related by $\omega/2\omega$. This harmonic relationship between the two frequencies permits the reuse of the microbunching generated in the first undulator array and minimizes interpulse jitter. The intensities of the pump and probe pulses were monitored by gas monitor detectors filled with krypton and nitrogen gas respectively. The fluctuation of the pump pulse intensity allows one to select pulses that yield low ionization fraction - and therefore create isolated ionization spur events. The pump-off spectra were obtained by filling the 15-m gas attenuator with argon gas, thus attenuating the pump beam to $1\%$ and the probe beam to $\sim 50\%$. The pump and probe beams transmitted through the liquid water sheet jet were energy dispersed on a 2D detector with a variable-line-spaced grating in order to monitor both the transient absorption spectrum and pump/probe alignment.

Figure 2 shows the transmission spectrum of liquid water obtained by a coordinated pump/probe scan with $\omega$ ($2\omega$) pulse durations of 700 (550) as. The bandwidth of the probe pulse was $\sim 5$ eV FWHM; the probe scan was conducted in 4 eV steps. Shot-by-shot spectra were accumulated

for 3 minutes at each energy to yield $> 10,000$ shots per step. Shots with median pump pulse energies of 19 $\mu$J ($3.4\mu$J on target) were selected to achieve photoinduced ionization fractions of $0.1\%$. The upper panel displays the pump-on and pump-off transmission spectra together with the liquid water absorption. The lower panel shows the differential absorption, $\Delta A$, for the minimum delay of 600 as. Two distinct regions are observed in the ATAS spectrum - the valence hole bands $1b_1$, $3a_1$, and $1b_2$ below 527 eV and the strong bleach signal near the pre-edge feature at 535 eV. Of importance is the observation of only a single $1b_1$ peak - an observation which persists at higher pump pulse energies.

As the first condensed phase AX-ATAS study we now establish the nature of the observed signal. Whereas the employed light pulses are confined to a sub-femtosecond timescale, the same does not hold, in general, for the response generated in the sample. The observed signal is complex due to contributions both from multichannel coherence and population dynamics (*9, 44, 45*). Moreover, since the attosecond soft x-ray–pump pulse may create holes anywhere in the entire valence band and collisional ionization by high-energy electrons plays a crucial role in the condensed phase, the overall dynamics are fundamentally different from those in isolated atoms or molecules. One may make a simple estimate of the importance of electron collisional ionization; the 235 eV photoelectron emitted after valence ionization with a 250-eV x ray can further ionize nearby water molecules with a cross-section given by $\sigma^{col} = 1/n_W\lambda$ where $n_W$ is the density of water molecules and $\lambda$ is the electron mean free path in water ($\sim$ 1.5 nm (*46*)). The kinetic energy of the photoelectron decreases with each collision such that after a certain number of collisional ionization steps the photoelectron no longer has sufficient energy to cause further ionization. The entire process can be viewed as a sequence of ionization steps, caused either by the photon (in the first step) or by the photoelectron (in all other steps) as illustrated in Fig. 1B.

The effects of collisional ionization, population dynamics and multichannel coherence on

the observed AX-ATAS signal were modeled in a microdomain containing 1000 water molecules (Fig. 3A). The calculations model the isolated ionization event scenario probed by experiment, i.e. a 0.1% photoionization probability. The methods are described in detail in the SM. Briefly, the pump-pulse-induced valence-hole population dynamics were computed using a rate-equation approach assuming a 0.7-fs pump pulse with a Gaussian temporal profile followed by the contribution from collisional ionization; both steps assumed equal ionization cross sections for all four valence orbitals. Following the formation of a single-hole state due to photoionization, the multiple-hole state populations rapidly build up as a consequence of collisional ionization by the photoelectron - on a subfemtosecond timescale. The probe pulse, a 0.55-fs Gaussian, arrives 0.6 fs later - while the sample is still undergoing collisional ionization. As shown in Fig. 3A, the polarization response, $P(t)$, detected in condensed phase AX-ATAS (green and pink lines), is confined to a temporal region much less than the core-hole lifetime expected for a gas-phase isolated system response (gray). The pump-induced polarization is strongly affected by dephasing by collisional ionization events and somewhat less by coherences between different valence holes ($1b_1$, $3a_1$, and $1b_2$) situated on the same O $1s$ core in the sample. In addition, the probe-induced polarization is confined, even at longer time delays, due to the continuous inhomogeneously broadened spectrum of the valence holes and large bandwidth of the probe pulse. The finding that the AX-ATAS response is confined to the sub-femtosecond timescale allows us to compute the observed transient absorption spectrum with static nuclei - even for liquid water where fast hydrogen atom vibrational motion is on the 10-femtosecond timescale.

The theoretical X-ray absorption spectra (XAS) were computed using multi-reference restricted-active-space configuration-interaction (MR-RASCI) (*47*) on tetrahedrally coordinated $(H_2O)_5$, as it is the simplest cluster mimicking the first solvation shell in “bulk water". The neutral and singly-ionized water pentamer represented the pump-off and pump-on species; their XAS were calculated to construct the $\Delta A$, as shown in Fig. 3B. Three types of transitions were calcu-

lated for O K-edge XAS: a) $1s$ electron excited into the hole vacancies of the primary water molecule; b) $1s$ electron excited into the unoccupied orbitals without any holes in the primary water molecule; c) $1s$ electron is excited into unoccupied virtual orbitals with a valence hole spectator. The calculated $\Delta A$ shown in Fig. 3B shows the expected valence-orbital holes (transition type a) and a pronounced bleach near 535 eV. The origin of the 535-eV bleach is Stark shifting of transitions from the O $1s$-core orbital to unoccupied orbitals that form the pre-edge feature due to the presence of a spectator valence hole in a neighboring water molecule. The line positions of the valence-orbital holes ($1b_1, 3a_1, 1b_2$) align with the experimental observations and support the labelling in Fig. 2. However, the agreement is not perfect as the calculated intensities assume that all valence holes have the same population - a condition that may not be met in the present measurement. The hole populations depend on the detailed cross sections of the photoionization and collisional ionization processes that give rise to those hole populations, i.e., the hole populations encode information on the ionization dynamics. We note that in both calculation and experiment a single $1b_1$ peak is obtained, suggesting that the assumed tetrahedral geometry may dominate the structural patterns present in room temperature water. Full calculation details are given in the SM for the pentamer as well as monomer and dimer species used to validate the methods.

We now compare our temporally confined AX-ATAS signal to previously measured x-ray emission (XES) spectra in liquid water (*33, 34*) and thus address the long-standing debate concerning the interpretation of the $1b_1$ doublet in the XES of liquid water (*24, 33, 34, 37, 38*). As shown in Fig. 4A, the two experimental methods couple equivalent core- and valence-hole states ($1s^{-1}$ and the $1b_1, 3a_1, 1b_2$) - but in reverse order. The emergence of the $1b_1$ doublet (commonly labelled $1b_1^{'}$ and $1b_1^{''}$) in XES of liquid water has been attributed to either (a) two structural motifs of liquid water or (b) ultrafast dissociation in the core-excited state. The latter is illustrated by data from recent theoretical investigations (*37, 38*) showing the evolution of the

XES within 4 fs due to proton dynamics. Both Theory A (*38*) and Theory B (*37*) calculate XES that evolves from a single $1b_1$ peak at $t = 0$ (upper panel Fig. 4C) to a doublet by 4 fs (lower panel Fig. 4C). Our AX-ATAS signal is confined to the sub-femtosecond timescale and thus eliminates contributions from ultrafast dissociation, whereas XES integrates nuclear dynamics over the core-hole lifetime of $\sim 4$ fs. Our experimental data show no evidence of the $1b_1$ doublet XES structure, which has a splitting of $\sim 1$ eV and a FWHM of $\sim 2$ eV as reproduced in the lower panel of Fig. 4B. (We would be sensitive to this doublet structure as the narrowest feature we observe is the $\sim 0.7$ eV-FWHM bleach.) In contrast, our data show a remarkable similarity to the theoretical data with frozen atomic positions at t= 0 fs shown in the upper panel of Fig. 4C. The discrepancy in the relative strength of the $3a_1$ and the $1b_1$ contribution may be attributed to the fact that the underlying mechanisms (collisional ionization + absorption vs. absorption + emission) are not completely identical. Our measurement thus provides unequivocal experimental evidence that the split peak does not originate from two structural motifs in liquid water - but rather highlights the importance of ultrafast proton dynamics when interpreting XES data.

In summary, we report the first all x-ray attosecond-pump attosecond-probe study in the important condensed phase target, liquid water. Analyzing the powerful all x-ray attosecond transient absorption spectroscopy method, AX-ATAS, we find that the temporal response in condensed phase is confined to a sub-femtosecond timescale. By freezing the motion of even the lightest atomic species, AX-ATAS overcomes a key limitation of the established XES technique. Specifically, the presented methodology allows us to suppress contributions to the probe signal from nuclear motion in inner-shell-excited states. In this way, we are able to isolate structural properties that are indicative of water in its ground electronic state, thereby resolving a long-standing debate surrounding the interpretation of the $1b_1$ x-ray emission doublet as being evidence for two structural motifs of ambient temperature liquid water. Moreover, our

experimental findings suggest that, more generally, AX-ATAS could become a powerful tool for investigating any condensed-matter system in which proton or hydrogen motion in probe-induced states can compromise the information content of the probe signal. We also note that this study, with tunable x-ray pump pulses, extends the range of phenomena studied by ATAS from light-induced processes, such as passage through conical intersections (*32*), to inner-shell processes at the heart of radiation damage. Indeed, the ability to take x-ray pump/probe spectral snapshots with sub-fs time resolution over a wide range of time delays, as enabled by arbitrary delays at an XFEL, will allow the study of the origin and evolution of reactive species produced by radiation-induced processes.

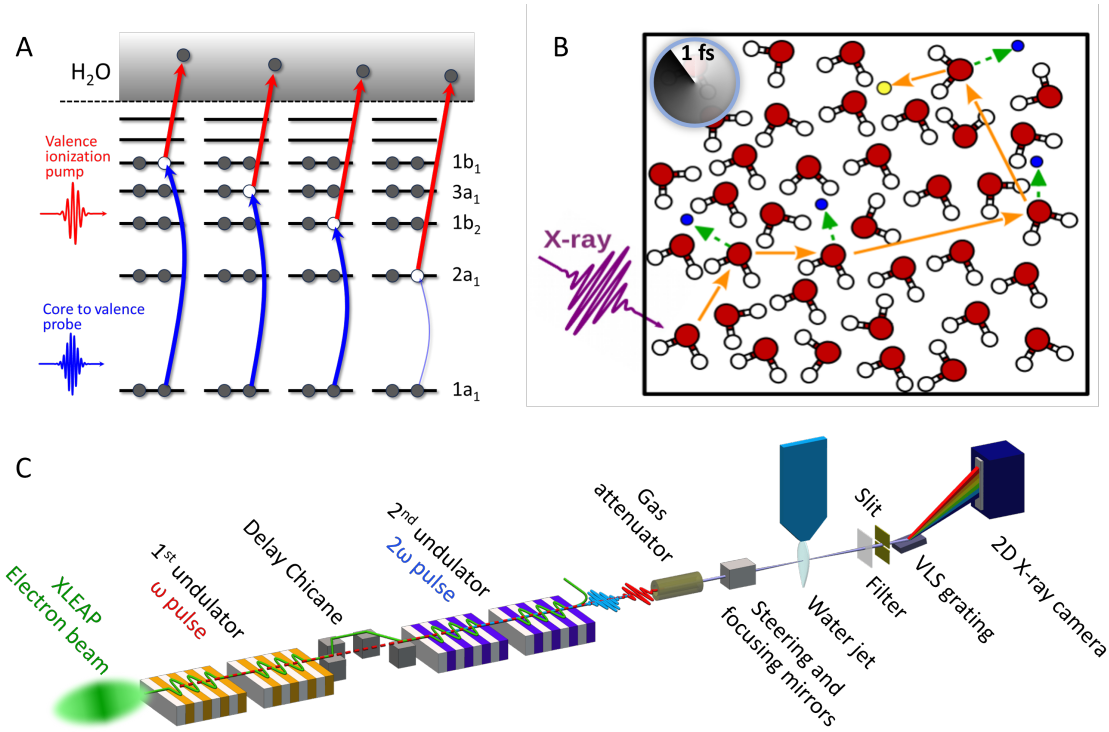


Figure 1: All x-ray probe attosecond transient absorption spectroscopy (AX-ATAS) in liquid water. Two synchronized attosecond pulses with photon energies related by $\omega/2\omega$ are incident on a water sheet jet and the transmitted $2\omega$ probe beam is energy dispersed onto a 2D camera. **(A)** The $\omega$ pulse has sufficient energy to ionize an electron from anywhere in the valence band while the $2\omega$ pulse probes the core-to-valence transition region near 530 eV. **(B)** Electrons resulting from the initial x ray-induced valence ionization go on to collisionally ionize nearby water molecules in the liquid phase sample on the sub-femtosecond timescale. **(C)** The first undulator array, tuned to $\omega$, imprints a microbunching that is reused in the second undulator array, tuned to $2\omega$, to produce an attosecond x-ray pulse pair with small interpulse jitter. (*30*)

.

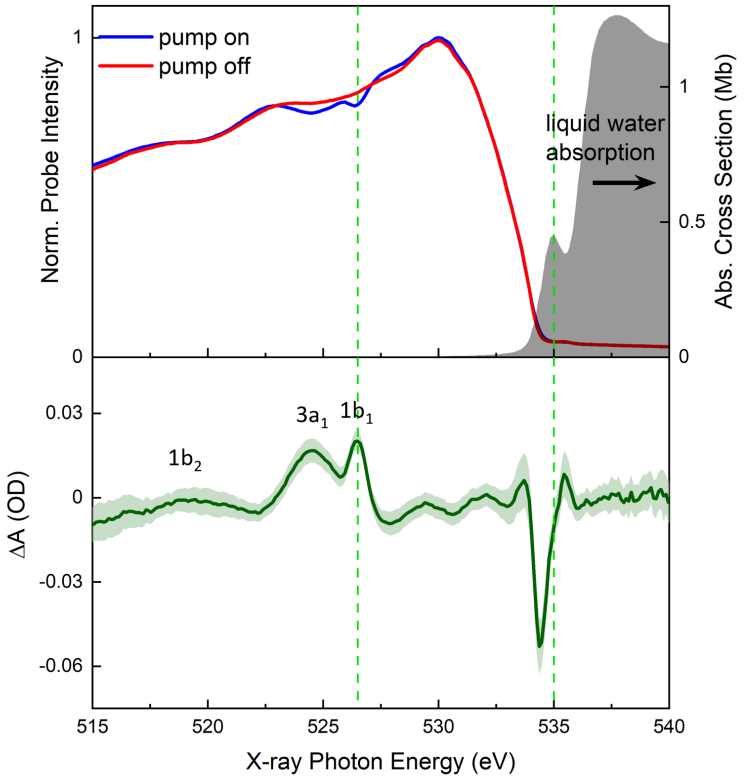


Figure 2: Upper: X-ray transmission spectra of the $2\omega$ probe pulse at 0.6-fs delay with (blue) and without (red) the 0.7-fs, $\omega$ pump pulse, with the water absorption spectrum shown in gray. Lower: Attosecond transient absorption spectrum ($\Delta A$) of liquid water covering the valence-hole and pre-edge region,.

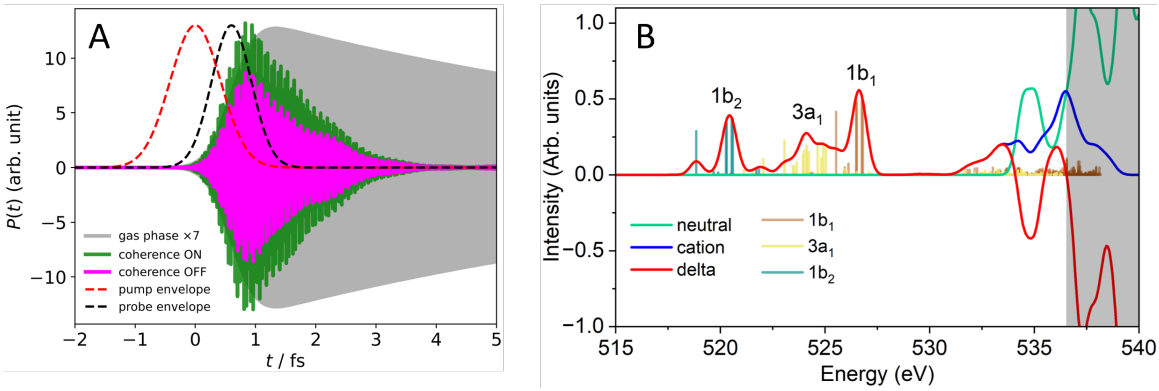


Figure 3: **(A)** Temporal confinement of the polarization response, $P(t)$, detected in the x-ray AX-ATAS signal - including effects due to collisional dephasing and multichannel coherences. **(B)** Multi-reference RASCI calculations of a water pentamer in neutral and singly ionized states to construct the change in absorption upon ionization, $\Delta A$, in the valence-hole and pre-edge region, with the liquid water absorption region shown in gray.

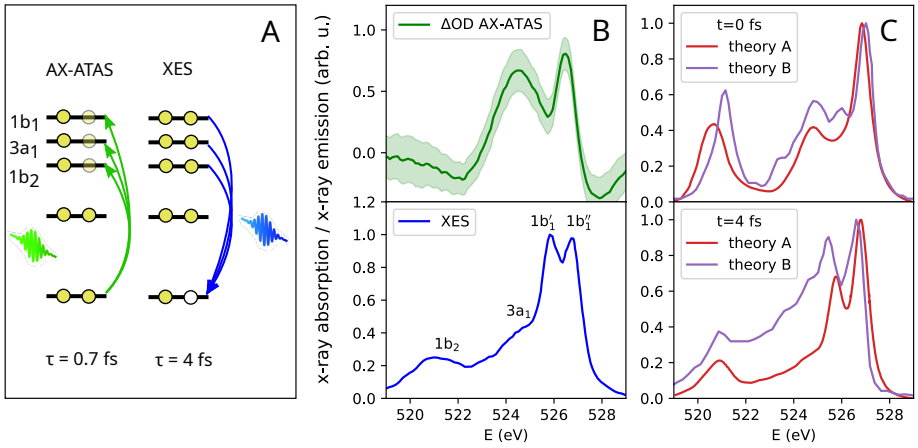


Figure 4: Comparison of all x-ray attosecond transient absorption spectra (AX-ATAS) and x-ray emission spectra (XES). **(A)** AX-ATAS and XES probe equivalent initial and final states. AX-ATAS: the pump pulse creates a hole anywhere in the valence band which the probe populates. XES: The O $1s$ hole is filled by emission from the entire valence band. **(B)** Upper: AX-ATAS spectrum, Lower: XES spectrum from liquid water (*33*). **(C)** Theoretical XES snapshots for liquid water. Upper: 0 fs, Lower: 4 fs. Theory A: Ref. (*38*) Fig. 3, Theory B: Ref. (*37*) Fig. 3

# References


1. Paul, P.-M. *et al.* Observation of a train of attosecond pulses from high harmonic generation. *Science* **292**, 1689–1692 (2001).

2. Hentschel, M. *et al.* Attosecond metrology. *Nature* **414**, 509–513 (2001).

3. Schultze, M. *et al.* Delay in photoemission. *Science* **328**, 1658–1662 (2010).

4. Isinger, M. *et al.* Photoionization in the time and frequency domain. *Science* **358**, 893–896 (2017).

5. Huppert, M., Jordan, I., Baykusheva, D., Von Conta, A. & Wörner, H. J. Attosecond delays in molecular photoionization. *Phys. Rev. Lett.* **117**, 093001 (2016).

6. Gong, X. *et al.* Attosecond spectroscopy of size-resolved water clusters. *Nature* **609**, 507–511 (2022).

7. Jordan, I. *et al.* Attosecond spectroscopy of liquid water. *Science* **369**, 974–979 (2020).

8. Cavalieri, A. L. *et al.* Attosecond spectroscopy in condensed matter. *Nature* **449**, 1029–1032 (2007).

9. Goulielmakis, E. *et al.* Real-time observation of valence electron motion. *Nature* **466**, 739–743 (2010).

10. Kraus, P. M. *et al.* Measurement and laser control of attosecond charge migration in ionized iodoacetylene. *Science* **350**, 790–795 (2015).

11. Sansone, G. *et al.* Electron localization following attosecond molecular photoionization. *Nature* **465**, 763–766 (2010).

12. Calegari, F. *et al.* Ultrafast electron dynamics in phenylalanine initiated by attosecond pulses. *Science* **346**, 336–339 (2014).

13. Ott, C. *et al.* Lorentz meets Fano in spectral line shapes: a universal phase and its laser control. *Science* **340**, 716–720 (2013).

14. Schultze, M. *et al.* Controlling dielectrics with the electric field of light. *Nature* **493**, 75–78 (2013).

15. Krausz, F. & Ivanov, M. Attosecond physics. *Rev. Mod. Phys.* **81**, 163 (2009).

16. Eckle, P. *et al.* Attosecond angular streaking. *Nat. Phys.* **4**, 565–570 (2008).

17. Leone, S. R. *et al.* What will it take to observe processes in'real time'? *Nat. Phot.* **8**, 162–166 (2014).

18. Tzallas, P., Skantzakis, E., Nikolopoulos, L., Tsakiris, G. D. & Charalambidis, D. Extreme-ultraviolet pump–probe studies of one-femtosecond-scale electron dynamics. *Nat. Phys.* **7**, 781–784 (2011).

19. Okino, T. *et al.* Direct observation of an attosecond electron wave packet in a nitrogen molecule. *Sci. Adv.* **1**, e1500356 (2015).

20. Fabris, D. *et al.* Synchronized pulses generated at 20 eV and 90 eV for attosecond pump–probe experiments. *Nat. Phot.* **9**, 383–387 (2015).

21. Popmintchev, D. *et al.* Near-and extended-edge x-ray-absorption fine-structure spectroscopy using ultrafast coherent high-order harmonic supercontinua. *Phys. Rev. Lett.* **120**, 093002 (2018).

22. Huang, S. *et al.* Generating single-spike hard x-ray pulses with nonlinear bunch compression in free-electron lasers. *Phys. Rev. Lett.* **119**, 154801 (2017).

23. Duris, J. *et al.* Tunable isolated attosecond x-ray pulses with gigawatt peak power from a free-electron laser. *Nat. Phot.* **14**, 30–36 (2020).

24. Nilsson, A. & Pettersson, L. G. The structural origin of anomalous properties of liquid water. *Nat. Comm.* **6**, 8998 (2015).

25. Loh, Z.-H. *et al.* Observation of the fastest chemical processes in the radiolysis of water. *Science* **367**, 179–182 (2020).

26. Svoboda, V. *et al.* Real-time observation of water radiolysis and hydrated electron formation induced by extreme-ultraviolet pulses. *Sci. Adv.* **6**, eaaz0385 (2020).

27. Garrett-Bakelman, F. E. *et al.* The NASA twins study: A multidimensional analysis of a year-long human spaceflight. *Science* **364**, eaau8650 (2019).

28. Alizadeh, E. & Sanche, L. Precursors of solvated electrons in radiobiological physics and chemistry. *Chem. Rev.* **112**, 5578–5602 (2012).

29. Garrett, B. C. *et al.* Role of water in electron-initiated processes and radical chemistry: Issues and scientific advances. *Chem. Rev.* **105**, 355–390 (2004).

30. Guo, Z. *et al.* Experimental demonstration of attosecond pump-probe spectroscopy with an x-ray free-electron laser. *Preprint* (2023).

31. Kobayashi, Y., Chang, K. F., Zeng, T., Neumark, D. M. & Leone, S. R. Direct mapping of curve-crossing dynamics in IBr by attosecond transient absorption spectroscopy. *Science* **365**, 79–83 (2019).

32. Zinchenko, K. S. *et al.* Sub-7-femtosecond conical-intersection dynamics probed at the carbon K-edge. *Science* **371**, 489–494 (2021).

33. Tokushima, T. *et al.* High resolution x-ray emission spectroscopy of liquid water: The observation of two structural motifs. *Chem. Phys. Lett.* **460**, 387–400 (2008).

34. Fuchs, O. *et al.* Isotope and temperature effects in liquid water probed by x-ray absorption and resonant x-ray emission spectroscopy. *Phys. Rev. Lett.* **100**, 027801 (2008).

35. Ball, P. Water—an enduring mystery. *Nature* **452**, 291–292 (2008).

36. Odelius, M. Molecular dynamics simulations of fine structure in oxygen K-edge x-ray emission spectra of liquid water and ice. *Physical Review B* **79**, 144204 (2009).

37. Takahashi, O., Yamamura, R., Tokushima, T. & Harada, Y. Interpretation of the x-ray emission spectra of liquid water through temperature and isotope dependence. *Phys. Rev. Lett.* **128**, 086002 (2022).

38. Cruzeiro, V. W. D., Hait, D., Shea, J., Hohenstein, E. G. & Martinez, T. J. 1b1 splitting in the x-ray emission spectrum of liquid water is dominated by ultrafast dissociation. *ChemRxiv* (2023).

39. Poole, P. H., Sciortino, F., Essmann, U. & Stanley, H. E. Phase behaviour of metastable water. *Nature* **360**, 324–328 (1992).

40. Woutersen, S., Ensing, B., Hilbers, M., Zhao, Z. & Angell, C. A. A liquid-liquid transition in supercooled aqueous solution related to the HDA-LDA transition. *Science* **359**, 1127–1131 (2018).

41. Kim, K. H. *et al.* Experimental observation of the liquid-liquid transition in bulk supercooled water under pressure. *Science* **370**, 978–982 (2020).

42. Debenedetti, P. G., Sciortino, F. & Zerze, G. H. Second critical point in two realistic models of water. *Science* **369**, 289–292 (2020).

43. Yun, Y., Khaliullin, R. Z. & Jung, Y. Correlated local fluctuations in the hydrogen bond network of liquid water. *J. Am. Chem. Soc.* **144**, 13127–13136 (2022).

44. Rohringer, N. & Santra, R. Multichannel coherence in strong-field ionization. *Phys. Rev. A* **79**, 053402 (2009).

45. Santra, R., Yakovlev, V. S., Pfeifer, T. & Loh, Z.-H. Theory of attosecond transient absorption spectroscopy of strong-field-generated ions. *Phys. Rev. A* **83**, 033405 (2011).

46. Sinha, N. & Antony, B. Mean free paths and cross sections for electron scattering from liquid water. *J. Phys. Chem. B* **125**, 5479–5488 (2021).

47. Jenkins, A. J., Hu, H., Lu, L., Frisch, M. J. & Li, X. Two-component multireference restricted active space configuration interaction for the computation of L-edge x-ray absorption spectra. *J. Chem. Theo. Comp.* **18**, 141–150 (2022).

48. Li, S. *et al.* Characterizing isolated attosecond pulses with angular streaking. *Opt. Exp.* **26**, 4531–4547 (2018).

49. Lutman, A. *et al.* Experimental demonstration of femtosecond two-color x-ray free-electron lasers. *Phys. Rev. Lett.* **110**, 134801 (2013).

50. Crissman, C. J. *et al.* Sub-micron thick liquid sheets produced by isotropically etched glass nozzles. *Lab on a Chip* **22**, 1365–1373 (2022).

51. Tillmann, B. *et al.* Imaging temperature and thickness of thin planar liquid water jets in vacuum. *Structural Dynamics* **10** (2023).

52. Champion, C. Electron impact ionization of liquid and gaseous water: a single-center partial-wave approach. *Physics in Medicine & Biology* **55**, 11 (2009).

53. Perry, C. F. *et al.* Ionization energy of liquid water revisited. *J. Phys. Chem. Lett.* **11**, 1789–1794 (2020).

54. Hao, Y., Inhester, L., Hanasaki, K., Son, S.-K. & Santra, R. Efficient electronic structure calculation for molecular ionization dynamics at high x-ray intensity. *Struct. Dyn.* **2**, 041707 (2015).

55. Pabst, S., Lein, M. & Wörner, H. J. Preparing attosecond coherences by strong-field ionization. *Phys. Rev. A* **93**, 023412 (2016).

56. Pabst, S. *et al.* Theory of attosecond transient-absorption spectroscopy of krypton for overlapping pump and probe pulses. *Phys. Rev. A* **86**, 063411 (2012).

57. Frisch, M. J. *et al.* Gaussian Development Version Revision J.24.

58. Herman, K. M. & Xantheas, S. S. An extensive assessment of the performance of pairwise and many-body interaction potentials in reproducing ab initio benchmark binding energies for water clusters n = 2 – 25. *Phys. Chem. Chem. Phys.* **25**, 7120–7143 (2023).

59. Pritchard, B. P., Altarawy, D., Didier, B., Gibsom, T. D. & Windus, T. L. A new basis set exchange: An open, up-to-date resource for the molecular sciences community. *J. Chem. Inf. Model.* **59**, 4814–4820 (2019).

60. Schwarz, J. *et al.* X-ray absorption spectroscopy of $H_3O^+$. *Phys. Chem. Chem. Phys.* **24**, 23119–23127 (2022).

61. Cavalleri, M., Ogasawara, H., Pettersson, L. & Nilsson, A. The interpretation of X-ray absorption spectra of water and ice. *Chem. Phys. Lett.* **364**, 363–370 (2002).

62. Boxer, S. G. Stark realities. *J. Phys. Chem. B* **113**, 2972–2983 (2009). PMID: 19708160.

# Acknowledgments

We thank R.W. Schoenlein for discussions leading to the experimental campaign and K. Kunnus for efforts in commissioning the ChemRIXS beamline. **Funding:** This work was primarily supported by IDREAM (Interfacial Dynamics in Radioactive Environments and Materials), an Energy Frontier Research Center funded by the U.S. Department of Energy (DOE), Office of Science, Basic Energy Sciences (FWP 68932). K.L. and G.D. acknowledge support by the U.S. Department of Energy, Office of Science, Basic Energy Science, Chemical Sciences, Geosciences and Biosciences Division under contract number DE-AC02-06CH11357. Use of the Linac Coherent Light Source (LCLS), SLAC National Accelerator Laboratory, and, resources of the Center for Nanoscale Materials (CNM), Argonne National Laboratory, are supported by the U.S. Department of Energy (DOE), Office of Science, Office of Basic Energy Sciences (BES) under Contracts DE-AC02-76SF00515 and DE-AC02-06CH11357. The effort from J.P.C. was supported by DOE, BES, Chemical Sciences, Geosciences, and Biosciences Division (CSGB). S.B., L.I., and R.S. acknowledge support from DESY (Hamburg, Germany), a member of the Helmholtz Association HGF. L.I. and R.S. further acknowledge support from the Cluster of Excellence 'CUI: Advanced Imaging of Matter' of the Deutsche Forschungsgemeinschaft (DFG) - EXC 2056 - project ID 390715994. **Author contributions:** L.Y., C.P. and R.S. originated the project concept. S.L., C.P., K.L., E.N, G.D., S.M., M.-F.L, D.J.H., D.G., G.Da., C.Y.H., J.K., K.La. and L.Y. executed the experiment and collected data. S.M. and M.-F.L. coordinated beamline reconfiguration. D.C., J.D., Z.Z. and N.S. setup and supported XLEAP attosecond configuration. J.C. and A.M. coordinated attosecond pulse-pair delivery. S.L, E.N. and R.D.S. characterized the target. S.L., K.L. and L.Y. analyzed experimental data. S.B., L.I., and R.S. provided supporting theoretical AX-ATAS modelling. L.L. and X.L. performed MR-RASCI

calculations. L.Y., R.S., S.L, L.L., S.B. and L.I. wrote the manuscript with input from all authors. **Competing interests:** None to declare. **Data and materials availability:** TBD

# Supplementary materials

Materials and Methods

Supplementary Text

Figs. S1 to S19

Tables S1

References *(48-62)*